Hyaluronic Acid-Polyethyleneimine Nanogels for Controlled Drug Delivery in Cancer Treatment

Emanuele Limiti,[a] Pamela Mozetic,[b] Sara M. Giannitelli,[a] Filippo Pinelli,[c] Xiaoyu Han,[d] Danila Del Rio,[e] Franca Abbruzzese,[a] Francesco Basoli,[a] Laura Rosanò,[e] Stefano Scialla,[a] Marcella Trombetta,[a] Giuseppe Gigli,[b,f] Zhenyu J. Zhang,[d] Emanuele Mauri,[a,] Alberto Rainer [a,b]***

[a] Department of Engineering, Università Campus Bio-Medico di Roma, via Álvaro del Portillo 21, 00128 Rome, Italy

[b] Institute of Nanotechnologies (NANOTEC), National Research Council, via Monteroni, 73100, Lecce, Italy

[c] Department of Chemistry, Materials and Chemical Engineering "G. Natta", Politecnico di Milano, via L. Mancinelli 7, 20131 Milan, Italy

[d] School of Chemical Engineering, University of Birmingham, Edgbaston, Birmingham B15 2TT, UK

[e] Institute of Molecular Biology and Pathology, National Research Council (CNR), Rome 00185, Italy

[f] Department of Mathematics and Physics "Ennio De Giorgi", Università del Salento, via per Arnesano, 73100 Lecce, Italy

* Emanuele Mauri. Tel.: +39 06225419627; fax: +39 06225419419; e-mail: e.mauri@unicampus.it

** Alberto Rainer. Tel.: +39 06225419214; fax: +39 06225419419; e-mail: a.rainer@unicampus.it

Abstract

The emulsion/evaporation method represents a pivotal approach to synthesize nanogels for controlled drug delivery. However, this strategy is constrained to the use of at least one polymer characterized by a phase-selective solubility in organic or aqueous solution. Consequently, the formulation of nanoscaffolds based on hydrophilic polymers only is not feasible by this approach, limiting the applicability of the technique. This work shows an innovative emulsion-based strategy where two polymers insoluble in water-immiscible organic solvents, hyaluronic acid (HA) and polyethyleneimine (PEI), chemically crosslink to produce nanogels. The adopted procedure exploits the interfacial interactions and the coalescence phenomena occurring in a surfactant-free mixed emulsion, composed of HA and PEI aqueous solutions as dispersed phases and a neat organic solvent as continuous phase. Our method allows to obtain HA-PEI nanogels characterized by low polydispersity, good colloidal stability, and high batch-to-batch reproducibility. The synthesized nanoscaffolds were validated as nanocarriers for the controlled release of doxorubicin in ovarian cancer, showing a sustained drug release profile (up to 15 days) which enhanced the therapeutic effects compared to the drug administration in free form. In particular, through an *in vitro* assay with a CD44 blocking/neutralizing antibody, we showed that the hyaluronan receptor was involved in the nanogel internalization process, suggesting that our nanogel formulation, obtained through a surfactant-free mixed emulsion, is a promising strategy for the design of HA-based nanocarriers for CD44 targeted therapy.

Keywords: nanogels, hyaluronic acid, mixed emulsion, controlled drug delivery, CD44, ovarian cancer

Introduction

In the last decade, research efforts have been dedicated to the development of nanocarriers targeted to enhance the delivery of drugs and achieve high therapeutic performances through the controllable release of the payload. Among them, nanogels (NGs) have attracted great attention thanks to their unique features, which strongly help to overcome the shortcomings of other drug delivery systems. They can be defined as nano-scaled hydrogels formed by physically or chemically crosslinked polymers which give rise to a three-dimensional (3D) tunable porous matrix with a high capacity to uptake large amounts of water or physiological fluids, while maintaining the internal network structure[1-2]. In particular, NGs appear as very promising candidates for nanomedicine compared to other nanoparticles, especially thanks to their high drug loading (up to 50% of their weight)[3]. Indeed, they can efficiently encapsulate therapeutics of diverse nature through either simple physicochemical mechanisms (generally driven by NG swelling), or drug absorption *via* formation of salt bridges, hydrogen bonding and dipole-dipole interactions with the nanoscaffold architecture. The former mechanism involves the elongation of the polymer chains in the presence of a liquid, which expands the nanostructure until elastic retroactive forces counterbalance the deformation of the system: in this way, drug loading can be efficiently performed exploiting the "sponge-like effect" of NGs, until a swelling equilibrium is reached in the aqueous medium. The latter is promoted by the high NG surface area, which enhances the multivalent interactions and the bioconjugation with the drug. These mechanisms of drug loading also highlight two more aspects: first, by decoupling NG synthesis and drug loading steps, potential drug inactivation under reaction conditions is avoided; second, the phenomena occurring in the drug loading phase counteract the burst release of the payload, which will be released in a more sustained and controlled manner, compared to other conventional polymer nanoparticles.

Furthermore, as widely discussed in the literature, NGs can be efficiently internalized by the target cells, thereby lowering the therapeutic dosage and minimizing harmful side effects[4-5]. An especially

attractive class of NGs is represented by hydrophilic networks synthesized *via* the so-called emulsification/solvent evaporation technique. This strategy relies on the formation of an emulsion[6]—either water-in-oil or oil-in-water—, with the following constraints: *i*) at least one of the two starting polymers has to be dissolved in a volatile organic solvent, that is immiscible with water, *ii*) the other hydrophilic polymer has to be dispersed in the aqueous phase. The polymer crosslinking takes place at the water-oil interface, avoiding bulk reactions, and forms a highly structured 3D nanonetwork. Finally, the resulting nanoscaffolds are collected following the evaporation of the organic solvent. As an example, the emulsion/evaporation method has led to the formulation of polyethylene glycol (PEG) and polyethyleneimine (PEI) nanogels, where PEG is activated with imidazole groups and dissolved in dichloromethane (the organic phase), whereas PEI is dissolved in water (the aqueous phase). The formation of NGs occurs through chemical crosslinking between PEG imidazole and PEI amine groups. Such NGs have been validated in different cancers[7] and neurodegenerative disorders[8]. A similar strategy has been developed using poloxamers (*i.e.*, block copolymers of poly(ethylene oxide) and poly(propylene oxide)), functionalized imidazole and PEI[9]. Additionally, nanoscaffolds have been also prepared using stearic acid and oleic acid at different ratios in an aqueous poloxamer solution to design an *in situ* mucoadhesive gel[10].

The emulsion/evaporation method is suitable to modulate size, shape, composition and surface properties of the NGs, by simply tuning the concentration of the polymers and the droplet size of the dispersed phase. However, the need to have one of the NG building blocks soluble in a water-immiscible organic solvent limits the range of eligible polymers and, as a consequence, the applicability of the technique. Indeed, the synthesis of these nanocarriers using hydrophilic polymers only cannot be carried out. An alternative strategy to address this limitation is represented by the micellar approach, which requires one component to form polymeric micelles in aqueous phase, exposing as external layer its reactive moieties for the crosslinking with a second polymer[9].

However, this approach is restricted to a limited range of polymer systems. To solve this challenge, in this work we propose a novel approach based on a herein defined mixed emulsion, where each of the two polymers constituting the NGs is separately dissolved in water, without the addition of surfactants and subsequently dispersed into the same continuous phase, made of an organic volatile solvent.

This innovative procedure eliminates the need to have one of the building blocks soluble in an organic solvent, immiscible with water, to obtain the nanoscaffold formation, enabling the synthesis of NGs based on hydrophilic polymers only.

We named the protocol Mixed Emulsion/Evaporation Technique (MEET).

In detail, we have applied this strategy to design NGs composed of hyaluronic acid (HA) and linear polyethyleneimine (LPEI), two polymers that are not soluble in water-immiscible organic solvents. HA is an anionic, non-sulfated glycosaminoglycan commonly used in the fabrication of biomaterials for tissue engineering, drug delivery and imaging purposes, due to its highly biodegradable, biocompatible, viscoelastic, non-toxic, and non-immunogenic nature[11-12]. Among the biological applications, HA has been widely investigated for target therapy in cancer, thanks to its well-demonstrated affinity to CD44 (hyaluronan receptor), overexpressed on the surface of many tumor cells[13]. For this reason, the polymer may act as an active targeting moiety for the intracellular delivery of anticancer drugs and represents a suitable component for the synthesis of nanocarriers[14-15]. On the other hand, LPEI is a cationic polymer widely used in the synthesis of nanocarriers for drug and gene delivery due to its unique proton-sponge effect[16-17]. The presence of amine groups in the polymer backbone enables its covalent coupling with several functionalities/biomolecules and the formation of 3D nanomatrices with a huge internal space and a soft skeleton structure. This results in an improved encapsulation efficiency of drug molecules, thanks to the electrostatic interactions with the LPEI positive charge density. Moreover, the potential cytotoxicity of neat LPEI is overcome by its conjugation with other polymers, thereby justifying its use in the design of nanoscaffolds[18].

The use of MEET for the synthesis of HA-PEI nanocarriers represents an advantageous alternative to other synthetic routes described in the literature for HA- or PEI-based nanoscaffolds. Indeed, our strategy requires few synthetic and purification steps to activate the polymers and form NGs, defining a straightforward and robust method. In the literature, HA-PEI nanoscaffolds are generally obtained through: *i)* activation of HA with aldehyde/disulfide moieties[19-20] and subsequent reaction with primary amines of branched PEI; *ii)* surface decoration of PEI-PEG, PEI-PLGA or PEI-PBAE pre-formed particles with HA chains[21-23]; or *iii)* formation of nanocomplexes *via* electrostatic interactions[24-25]. Overall, these procedures involve multiple orthogonal activation routes, longer reaction times and the use of larger volumes of water and organic solvents. Furthermore, the nanocarriers obtained by the above methods preferentially result in a core-shell configuration, characterized by a sectorial and inhomogeneous distribution of the different polymer chains in the nanonetwork, which could affect their drug delivery and cell uptake performance. Our MEET approach, exploiting the emulsion/evaporation principles, allows us to obtain homogeneous HA-LPEI NGs characterized by the combination, within a single nanoscaffold, of both physical (by HA) and electrostatic (by LPEI) interactions with the payload, coupled to HA-mediated affinity toward cancer cells and PEI-mediated endosomal escape[26].

The NGs obtained by MEET were characterized in terms of size, morphology and surface charge, and loaded with doxorubicin (a known antiblastic drug) to validate their potential application as a therapeutic delivery system in ovarian cancer, using the cell line OVCA433 as a representative model of cancers overexpressing CD44. Through a competitive assay, we could demonstrate an involvement of CD44 in the NG internalization process. We also documented that the NG-mediated delivery of doxorubicin (DOX) significantly affected the metabolic activity of target cells, outperforming the conventional DOX administration route in the form of a non-encapsulated drug.

Hence, this study demonstrates a convenient route for NG synthesis, which extends the applicability range of conventional emulsification/solvent evaporation methods to more classes of biopolymers,

including the design of nanocarriers based on hydrophilic polymers. In addition, the study validates the obtained NGs as CD44-targeting drug delivery nanocarriers for cancer treatment.

Experimental Section

Materials

Hyaluronic acid sodium salt (HA, ultra-low Mw=8–15 kDa) was purchased from Biosynth Carbosynth (Compton, UK) and linear polyethyleneimine (LPEI Mw=2.5 kDa) from Polysciences Inc. (Warrington, USA). Doxorubicin was purchased form Teva Italia S.r.l. (Milan, Italy). All other chemicals were purchased from Merck KGaA (Darmstadt, Germany) and used as received, without any further purification. Solvents were analytical grade. Cy5-derivatives were stored at -20 °C.

LPEI functionalization with Cy5 (LPEI-Cy5)

LPEI and Cy5 were crosslinked according to a two-step procedure discussed in a previous work[27]. The first stage concerned the modification of LPEI with alkyne groups: the polymer (250 mg, 0.1 mmol) was dissolved in methanol (7 mL), and 80 wt% propargyl bromide solution in toluene (108 μL, 1 mmol) was added dropwise at 0 °C. The resulting solution was kept under stirring for 24 h at room temperature (RT) in the dark. Methanol was evaporated under reduced pressure, and the resulting viscous intermediate was redissolved in deionized water (DIW). The solution was purified by membrane dialysis against distilled water (dialysis membrane MWCO = 100–500 Da) for 2 days, with daily water exchange, and the alkyne-modified LPEI collected as a solid after freeze-drying. In the second stage, the copper(I)-catalyzed alkyne-azide cycloaddition (CuAAC) occurred: functionalized LPEI (220 mg, 0.088 mmol) was dissolved in DIW (10 mL) and Cy5-azide (200 μL, 2 mg/mL in DMSO) was added dropwise to the system. The copper catalyst ($CuSO_4$, 13 μg, 0.08 μmol) and sodium ascorbate (16 μg, 0.08 μmol) were added to the mixture, which was left under stirring for 36 h at 50 °C in the dark. The product was dialyzed (membrane MWCO = 100–500 Da)

against DIW for 2 days with daily water exchange to remove unreacted species. The final LPEI-Cy5 was collected after freeze-drying.

Nanogel synthesis

The nanogel synthesis involved the use of aqueous solutions of HA and LPEI. HA (10 mg) was dissolved in DIW (2 mL) and the coupling agents *N*-(3-dimethylaminopropyl)-*N′*-ethylcarbodiimide hydrochloride (EDC, 22.66 mg, 0.12 mmol) and *N*-hydroxysuccinimide (NHS, 5.56 mg, 0.048 mmol) were added to the polymer solution, at a molar ratio HA carboxyl groups:EDC:NHS 1:5:2. The reaction system was kept under stirring for 3 h at RT. Pristine LPEI and LPEI-Cy5 (1 mg, 1:1 by weight) were dissolved in 1 mL dilute HCl (pH = 4.5). The polymer crosslinking reaction occurred as follows: dichloromethane (DCM, 3 mL) was added dropwise to the activated HA solution and sonicated for 30 min, generating the first W/O emulsion. Then, the LPEI solution (*i.e.,* pristine LPEI and LPEI-Cy5) was added dropwise to the system and the final mixture was further sonicated for 15 min, generating a mixed emulsion of two disperse aqueous phases and a continuous organic one. This emulsified system was left under vigorous stirring overnight, at RT, allowing the organic solvent to evaporate. Finally, it was dialyzed against distilled water (membrane MWCO = 6–8 kDa), for 2 days with daily water exchange, freeze-dried and collected as a sponge-like solid. The HA:LPEI ratio of the present formulation was chosen following a preliminary evaluation of NG size and cytotoxicity as described in Supplementary Information.

NMR and IR analysis

Starting materials, intermediates and final nanoscaffolds were analyzed by Nuclear Magnetic Resonance (^{1}H NMR), carried out on a Bruker AC (400 MHz, Bruker Corp., Billerica, MA) spectrometer using deuterium oxide (D_2O) as deuterated solvent, and the chemical shifts were reported as δ values (ppm) relative to tetramethylsilane (TMS) internal reference compound. Further characterizations were performed by Attenuated Total Reflectance Fourier Transform InfraRed spectroscopy (ATR/FTIR), using a Thermo Nexus 6700 spectrometer coupled to a

Thermo Nicolet Continuum Infrared microscope equipped with a 15 × Reflachromat Cassegrain objective (Thermo Fisher Scientific, Waltham, MA) in the wavenumber range 4000–800 cm^{-1}, with 32 accumulated scans and at a resolution of 4 cm^{-1} for each specimen.

Dynamic light scattering (DLS) analysis

The final size, the polydispersity index (PDI) and the ζ-potential of nanogels were determined by DLS analysis (Zetasizer Nano ZS, Malvern Panalytical, Malvern, UK) in PBS, acid (pH = 4.5) and basic (pH = 8.5) solutions. Specimens were prepared at a concentration of 1 mg/mL and sonicated to ensure the complete dispersion in the medium, minimizing potential aggregates. Additionally, NG enzymatic degradation was evaluated using a solution of hyaluronidase from bovine testes (HAase, 400-1000 U/mg solid) at two different specific activities of 10 U/mL and 150 U/mL: according to literature[28-29], NGs were dispersed (1 mg/mL) in 0.1 M sodium acetate buffer plus 0.15 NaCl containing BSA (1 mg/mL) and HAase, at 37 °C. At defined time points, the effective hydrodynamic diameter and light scattering intensity of the NG suspensions were monitored *in situ*. Readings were performed in triplicate.

Atomic force microscopy (AFM) analysis

AFM measurements were carried out using a Dimension 3100 AFM with a Nanoscope III controller (Veeco Instruments Inc., Cambridge, UK) fitted with gold cantilevers (NanoWorld Pointprobe®), in contact mode with a spring constant of 0.08 $N \cdot m^{-1}$. The specimen was resuspended in distilled water at a concentration of 0.5 mg/mL, sonicated for 10 min at 20 °C, and dropped (2 μL) on Thermo polysine slides (Thermo Fisher Scientific), until reaching the evaporation of the solvent on the substrate at RT. AFM images on 30 × 30 μm areas were recorded for the preliminary morphologic evaluation, followed by the analysis of 4 × 4 μm ROIs.

Scanning electron microscopy (SEM)

NG specimen was prepared as described in the previous section on mica sheets and sputter coated with platinum. A field-emission SEM (FEI XL 30 ESEM-FEG, Thermo Fisher Scientific) scanning was performed at an accelerating voltage of 10 kV with SE (secondary electrons) detection mode.

Transmission Electron Microscopy (TEM)

Morphology of NGs, both as-synthesized and following enzymatic degradation, was evaluated by TEM (FEI Tecnai G2 Microscope, Thermo Fisher Scientific). NG suspensions were diluted to a final concentration of 250 μg/mL in DIW and 3 μL were dropped on a lacey carbon coated 300 mesh copper grid (Agar Scientific Stansted, Essex, UK), followed by dehydration at 50 °C until complete solvent evaporation. TEM micrographs were recorded at an accelerating voltage of 120 kV.

Drug loading

Doxorubicin (DOX) was chosen as a representative drug to evaluate the performance of the synthesized nanocarrier in terms of encapsulation and controlled release of therapeutics. DOX loading was performed in PBS (pH=7.4), as follows: 30 μL of a 100 μM DOX solution were added to the lyophilized specimens (3 mg) and samples were centrifuged for 15 s at 6000 rpm. Then, the system was left at RT for 15 min to complete the uptake of DOX. Finally, the resulting loaded nanocarriers were dialyzed (membrane MWCO = 3.5 kDa) against PBS for 30 min, in order to remove the non-absorbed drug. The encapsulation efficiency (EE %) was estimated according to the following equation (Eq. (1)):

$$\mathrm{EE\%} = \frac{DOX_{NG}}{DOX_{tot}} \cdot 100\% = \frac{DOX_{tot} - DOX_{sol}}{DOX_{tot}} \cdot 100\% \qquad (1)$$

where DOX_{NG} represents the encapsulated fraction and DOX_{sol} the residual unabsorbed fraction of the total drug payload (DOX_{tot}). DOX_{sol} was determined by fluorescence spectroscopy (λ_{ex} = 488

nm; λ_{em} = 590 nm) of withdrawn aliquots (3 × 100 μL) at defined time points, based on a DOX standard calibration curve (Supporting Information).

Drug release profile

The DOX-loaded nanosystems were diluted to a final concentration of 10 mg/mL and 100 μL of nanogel suspension were allowed to exchange against PBS (0.6 mL) at 37 °C. At defined time points, 100 μL aliquots were withdrawn and spotted into 96-well plates for fluorescence spectrophotometric analysis. At each withdrawal, elution buffer was replenished with fresh PBS to avoid mass transfer equilibrium between the nanosystem and the surrounding solution. Cumulative percentage of released DOX was estimated by fluorescence spectroscopy at λ_{ex} = 488 nm and λ_{em} = 590 nm, according to the drug calibration curve. Additionally, drug release studies were performed in acidic (pH = 4.5, representative of the pH levels in the stomach[30]), alkaline (pH = 8.5, as a threshold value which can be reached in the diseased intestine[31]) and HAase-containing solutions. Experimental data were collected from three independent replicates and reported as mean ± standard deviation (SD).

Cell cultures

Human epithelial ovarian cancer cell line OVCA433 was obtained from the American Type Culture Collection (ATCC) (LGC Standards, Teddington, UK). OVCA433 cells were cultured in Dulbecco's modified Eagle medium (Cat# 21885-025, GIBCO Thermo Fisher Scientific), supplemented with 10% fetal bovine serum, 50 units/mL penicillin and 50mg/mL streptomycin. Cells were incubated at 37 °C in a humidified atmosphere with 5% CO_2.

Cell viability and NG biocompatibility

Cell viability in the presence of NGs was assessed using Vybrant cytotoxicity assay kit (Thermo Fisher Scientific) according to the manufacturer protocol. NGs were suspended in culture medium (20 μg/mL) and administered to OVCA433, 24 h after their seeding at a density of 1.5 $\times 10^4$

cells/cm^2. 50 μL of supernatant were transferred into a 96-well plate and, after 10 min of incubation with 50 μL of resazurin/reaction mixture at 37 °C in 5% CO_2, the fluorescent metabolite of resazurin (resorufin) was detected (λ_{ex} = 530 nm; λ_{em} = 590 nm) on an Infinite M200-Pro multiplate reader (TECAN, Männerdorf, Switzerland). The release of the cytosolic enzyme glucose 6-phosphate dehydrogenase (G6PD) from damaged cells into the surrounding medium was quantified after 2, 6, and 24 h. The measured fluorescence is proportional to the amount of G6PD released into the medium, which is correlated to dead cells in each specimen. Each experiment was performed in triplicate for each time point, and viability levels were normalized to the control (*i.e.*, fully lysed cells).

Flow cytometric analysis

The selectivity of the NGs for CD44 and the involvement of hyaluronan receptor in the internalization process were studied. OVCA433 cells were seeded at a density of 1.5×10^4 cells/cm^2 into 12-well plates for 24 h and CD44 was blocked with an anti-CD44 blocking/neutralizing antibody (clone IM7, PE-Cy7 labeled; Thermo Fisher Scientific). Briefly, cells were washed in PBS and incubated for 45 min at RT with the antibody (1.25 ng/μL in PBS). Then, cells were washed in PBS (3 times) and NGs were administered at a final concentration of 20 μg/mL. Control group was represented by OVC433 cells without CD44 blocking treatment. At 2, 6, and 24 h time points, cells were analyzed by flow cytometry (CytoFLEX flow cytometer, Beckman Coulter, Brea, CA) with CytExpert software (Beckman Coulter). Living cells were gated on a forward vs. side scatter (FSC/SSC) dot plot; NG signal was recorded in the allophycocyanin (APC-A700) channel and quantified as the median fluorescence intensity (MFI) fold change at each time point. Fluorescence compensation was applied to correct the fluorescence spillover of Cy5 (NGs) and Cy7 (antibody) dyes.

Fluorescence staining and confocal microscopy analysis

The cellular internalization of NGs was also visualized using confocal microscopy. OVCA433 cells were seeded at a concentration of 1.5×10^4 cells/cm^2 into μ-Slide 8 well high Glass Bottom (Ibidi GmbH, Gräfelfing, Germany) for 24 h, while CD44 blocking and NG uptake were performed as described in the previous section. After 24 h, cells were fixed in paraformaldehyde (4% in PBS) for 15 min at RT, then incubated for 5 min in Triton X-100 (0.1% in PBS) to permeabilize cell membranes. Subsequently, they were washed 3 times in PBS, incubated with ActinGreen 488 stain (GeneCopoeia, Rockville, MD; 1:80 dilution in PBS for 40 min, in the dark), washed in PBS (3 times), and counterstained with DAPI (Thermo Fisher Scientific; 1:1000 dilution in PBS for 10 min, in the dark). Micrographs were collected using a Nikon A1R+ laser scanning confocal microscope (Nikon Instruments, Tokyo, Japan) with a 20× NA1.0 air objective.

Cell-assay of NG-mediated DOX delivery

Cell metabolic activity was evaluated following the administration of DOX-loaded NGs to validate their potential therapeutic effect. OVCA433 were seeded at a density of 1.5×10^4 cells/cm^2 in growth medium and incubated for 24 h. Then, DOX-loaded NGs (DOX-NG, 5.8 ng DOX per mg NG) were added to cells at a concentration of 20 μg/mL. Cells incubated with pristine (i.e., non-encapsulated) DOX represented the control group. All conditions were set to achieve the same final concentration of 0.2 μM drug in culture medium. MTT assay was used according to the manufacturer instructions. Briefly, activity of mitochondrial dehydrogenases in living cells was measured in terms of absorbance at 570 nm (TECAN Infinite M200-Pro) after 3 h exposure to a 0.5 mg/mL MTT solution in PBS, at 37 °C and 5% CO_2. Absorbance values obtained in the absence of cells were used for background subtraction. Untreated cells were used as a control for normalization. Experiments were performed in triplicate at different time points (24 h, 48 h, 72 h and 1 week).

Statistical analysis

Experimental data were analyzed using Prism ver. 9.3.0 (GraphPad Software, San Diego, CA) and reported as mean ± SD if not otherwise specified. One-way analysis of variance (ANOVA) followed by Tukey's multiple comparisons test was used to assess statistical significance, which was set at the 0.05 level.

Results and Discussion

Chemical characterization of nanogels

HA-LPEI nanogels were synthesized in a surfactant-free emulsion, consisting of two polymeric solutions of HA and PEI as aqueous dispersed phases, and a continuous organic one. This multiphase system is much more versatile than standard emulsion-based strategies, because none of the starting polymers needs to be soluble in an organic solvent, immiscible with water, to give rise to the crosslinking reaction (this prerequisite is binding in the conventional emulsion-based synthesis, which needs an organic-soluble and a water-soluble polymer). Our approach significantly extends the applicability of previous synthetic procedures based on conventional single (W/O or O/W) and multiple (W/O/W or O/W/O) emulsions[32-33], by leveraging the interactions between droplets of the two aqueous phases, driven by interfacial cohesion forces. In our procedure, the chemical crosslinking between HA and LPEI occurs at the droplet-droplet interface and the formation of the 3D nanoscaffold is completed upon droplet coalescence, exploiting the Brownian and Van der Waals interactions of the two polymer-containing disperse phases[34].

In detail, the proposed MEET protocol (Figure 1) involved the preparation of a first W/O emulsion of HA in DCM by sonication, followed by the addition of the LPEI aqueous phase, again under sonication. This mixed emulsion is characterized by the absence of surfactants, avoiding potential side-reactions in the formation of the NG scaffolds. The reaction between HA NHS-ester intermediate and LPEI amine groups gave rise to the final nanoscaffolds, which were collected in a single aqueous phase, after the evaporation of the organic solvent.

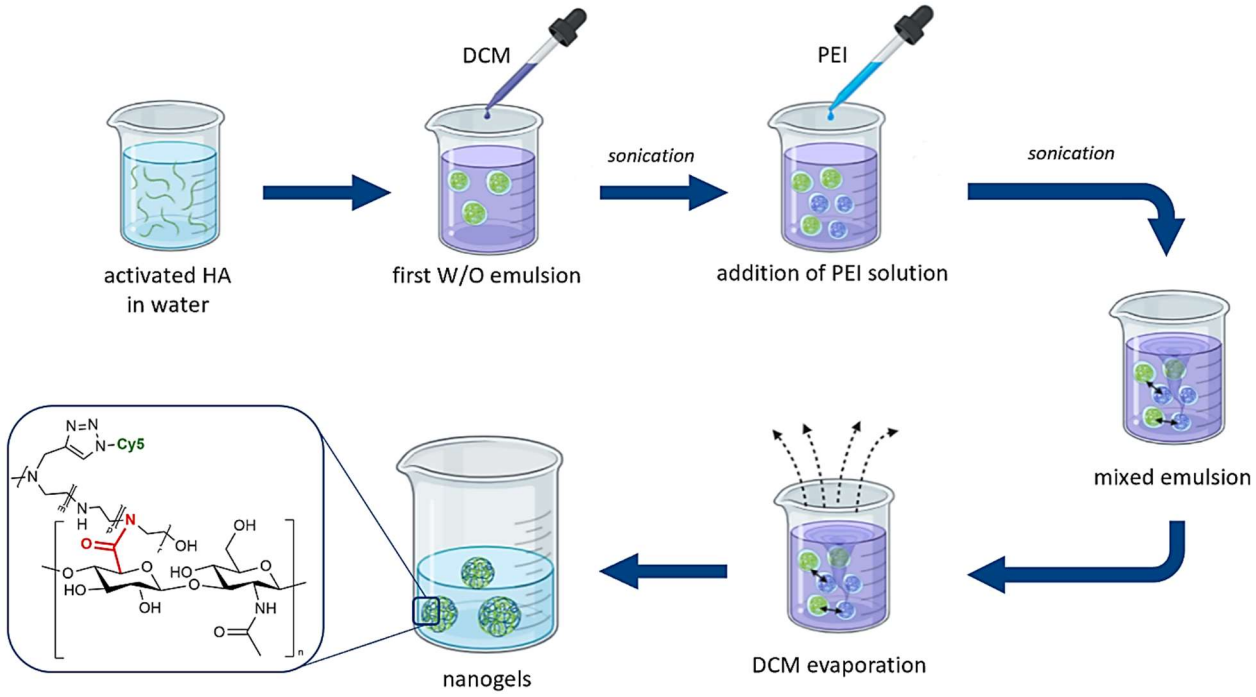

Figure 1. Scheme of NGs synthesis through MEET (Mixed Emulsion/Evaporation Technique). On the left: putative representation of the forming NG structure where the amide bond is highlighted (in red).

The Cy5 conjugation on PEI chains (characteristic triazole peak at 8.05 ppm[35]) and the formation of NGs were confirmed by ^{1}H-NMR analyses. In particular, in Figure 2, the amide crosslinking between HA and LPEI was proved by the shift of the signals ascribable to the methylene protons (N-*CH*$_2$-CH$_2$, *D*) of PEI monomer and the methine group (*CH*-COOH, *E*) of the HA ring moiety, involved in the reaction: the former was detectable at 3.38 ppm (signal at 2.93 ppm in the spectrum of neat LPEI) and the latter at 3.62 ppm (shoulder signal at 3.80–3.70 ppm in the HA spectrum). Moreover, the characteristic peak of HA methyl groups and of PEI backbone were clearly detectable, at 2.00 ppm and 2.85 ppm, respectively[36-37]. An estimation of the HA:PEI molar ratio in the nanoscaffold was conducted considering the integral values of their characteristic peaks and it resulted in HA:PEI 6:1, approximately.

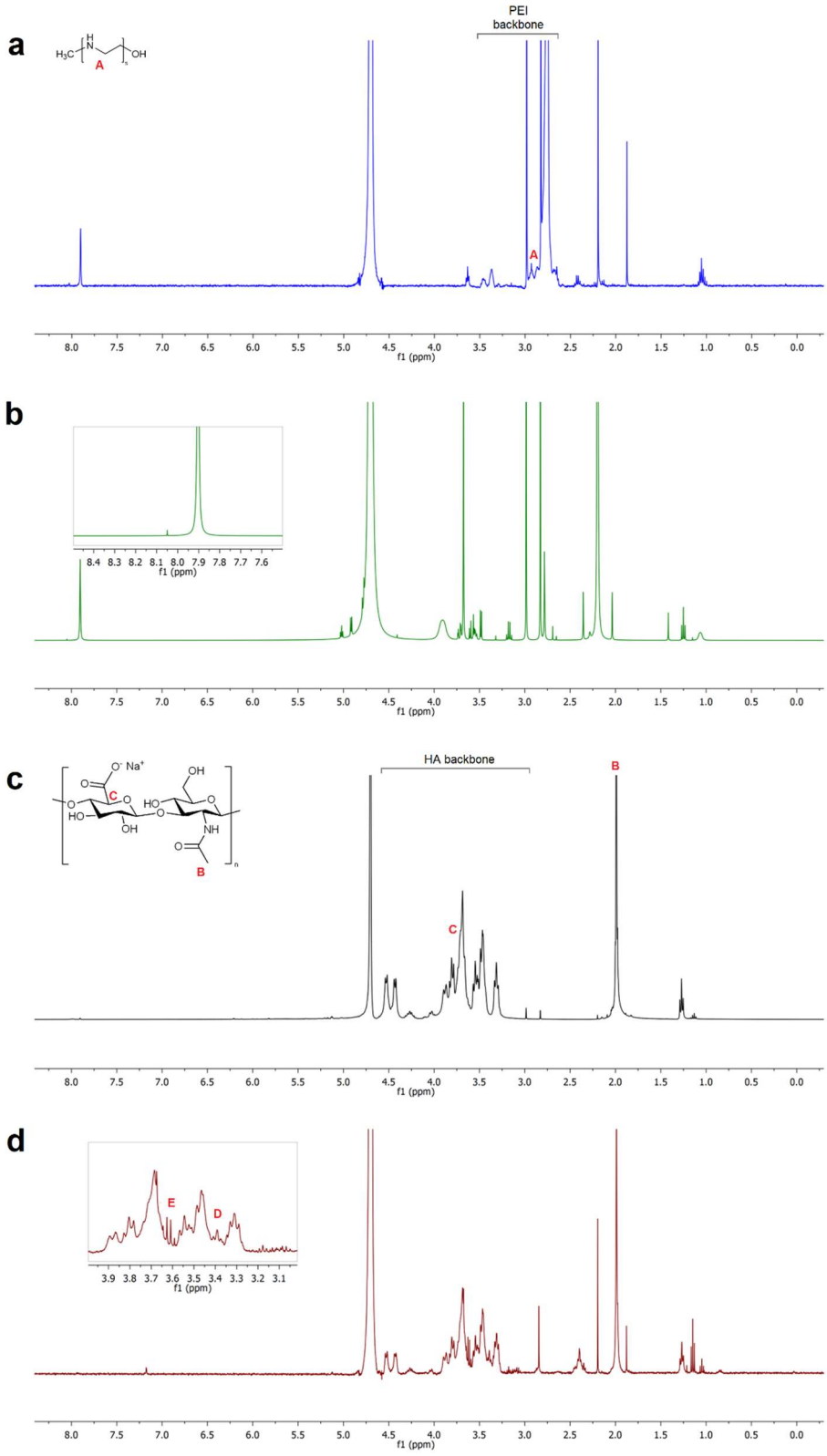

Figure 2. [1]H-NMR spectra of LPEI (a, blue; due to the different protonation degree of amino groups in the polymer backbone, A is indicative of the methylene protons subsequently involved in the crosslinking reaction); LPEI functionalized Cy5 (b, green); HA (c, black); and NGs (d, red). The signals of HA-LPEI crosslinking are highlighted.

The synthetic route leading to NG formulation was also monitored through FT-IR analysis, as shown in Figure 3. In detail, HA spectrum (Figure 3a) presented the following characteristic peaks: –OH stretching at 3296 cm^{-1}, aliphatic C–H stretching at 2880 cm^{-1}, carboxylic carbonyl stretching at 1739 cm^{-1}, amide II C=O stretching at 1608 cm^{-1} and C–H bending at 1407 cm^{-1} and 1376 cm^{-1}, C–CH_3 amide stretching at 1315 cm^{-1}, and the bands related to the stretching C–O–C bridge and the skeletal vibration involving the C–O stretching at 1148 cm^{-1} and 1040 cm^{-1}, respectively[38]. The LPEI spectrum (Figure 3b) showed the signal of –OH stretching at 3366 cm^{-1} and the stretching vibration of the aliphatic C–H at 2879 cm^{-1}, N–H bending at 1609 cm^{-1}, C–H bending and C–N stretching vibrations in the wavenumbers range 1450÷900 cm^{-1}. The conjugation of Cy5 on the PEI backbone (Figure 3c) was confirmed by the triazole linkage, ascribable to the signals at 1442 cm^{-1}(*) and 1461 cm^{-1}(**), and by the cyanine peaks around 2880 cm^{-1} and in the wavenumbers range 1500 ÷ 800 cm^{-1}, partially overlapped to PEI signals. Finally, the NG spectrum (Figure 3d) showed the characteristic signal of C=O stretching of the amide bond at 1731 cm^{-1} (†), representative of the successful HA-LPEI covalent crosslinking and the consequent nanoscaffold formation, besides showing all the characteristic peaks of the starting polymers.

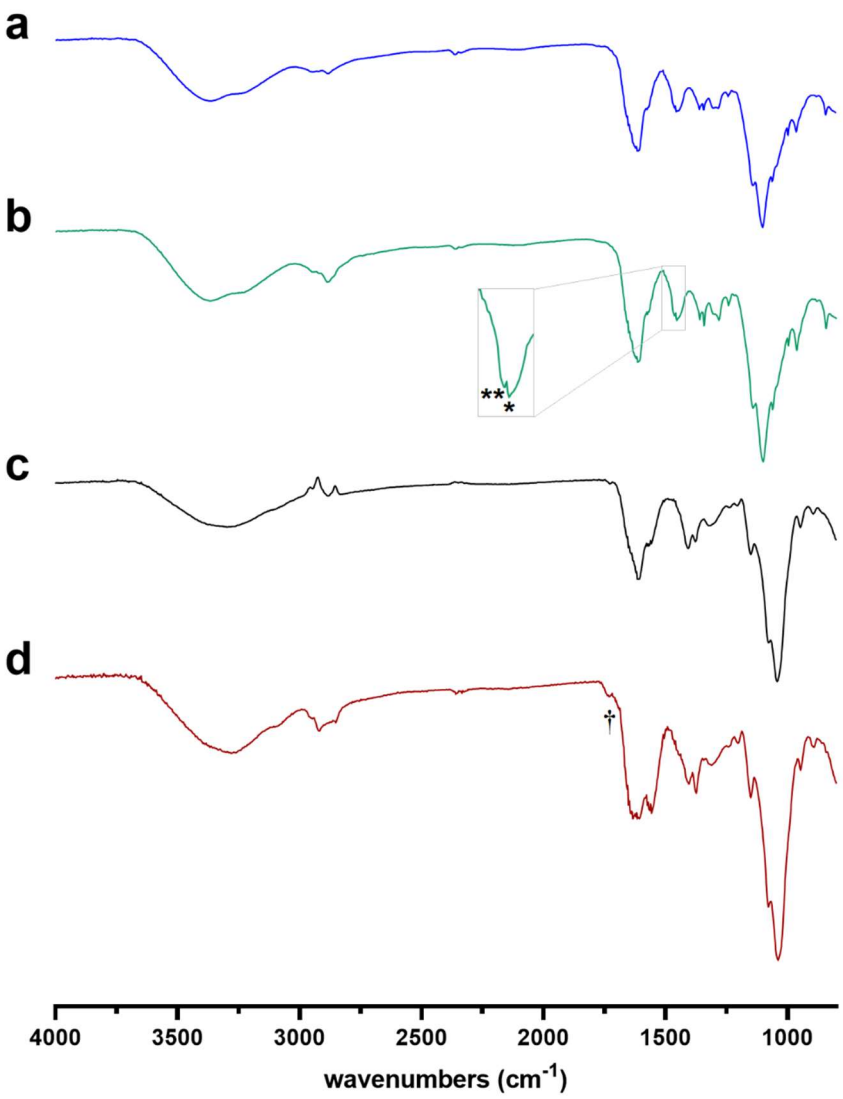

Figure 3. FT-IR spectra of LPEI (a, blue), LPEI functionalized Cy5 (b, green), HA (c, black) and NGs (d, red).

Physical characterization of nanogels: size and stability

The evaluation of NG size was conducted through DLS, AFM, SEM and TEM analyses (Figures 4a, 4b and 5c). DLS measurements of the hydrated NG specimens were carried out in different conditions (PBS, acidic and basic solutions) to investigate potential variations in NG size and their stability over time. In PBS medium, we recorded a mean hydrodynamic diameter of *ca*. 220 nm (polydispersity index PDI = 0.204) and a ζ-potential value of *ca.* – 8.7 mV. Additionally, NG stability was characterized by an initial phase of swelling due to the on-going hydration of the lyophilized specimen, followed by an equilibrium state with the surrounding environment (which

resulted in an almost constant NG diameter from the 24 h time point). Said initial swelling (maximum hydrodynamic diameter of 292.6 nm) was paralleled by a corresponding peak in the NG negative surface charge (-9.6 mV), suggesting a correlation between the two entities. Considering the HA:LPEI 6:1 molar ratio in NGs, the higher amount of negatively charged HA dictated the physicochemical behavior of the nanosystem. Indeed, as well documented in the literature, HA is characterized by solvation and diffusion of molecules/ions toward the polymer backbone at a faster rate than the polymer chain relaxation[39]: this resulted in an increased hydration effect and in an expanded polymer conformation with larger end-to-end distance (overshoot value); when this elongation is counterbalanced by the polymer chain reactive force, some of the absorbed molecules are forced out of the HA network, and an equilibrium state is achieved[40-41]. In parallel, this behavior supported the maximization of the overall electrostatic and polar interactions between the HA functional groups and the ionic species, providing a slight increase in the value of the negative electrical double layer associated to the nanostructure, until the equilibrium condition. After drug encapsulation, a slight variation in NGs size was recorded (Supporting Information), attributable to the steric hindrance of the entrapped drug and its physico-chemical interaction with the polymer chains: however, this difference can be considered not relevant in terms of cellular uptake[35].

Furthermore, NG stability was also tested in acidic (pH 4.5) and basic (pH 8.5) solutions: a moderate increase in plateau diameter was observed in both conditions, suggesting no aggregation and a good stability. The pH-dependent variations in hydrodynamic diameters could be ascribed to the different ionic nature of the polymers: PEI exhibits the highest protonation degree at pH 4.5, whereas it is substantially deprotonated in alkaline conditions[42-43]; on the other hand, HA is characterized by a lower net negative charge in acidic *vs.* basic medium and a decreasing radius of gyration at alkaline pH values[44-45]. As a result, at pH 4.5, the prevailing PEI positive charge density gives rise to repulsion forces between the protonated residual amino groups, favoring the increase in NG size (*ca.* 80 nm increase in hydrodynamic diameter); in alkaline conditions, the HA ionic

strength and the electrostatic repulsion between its carboxyl and hydroxyl groups favors an elongated configuration of the polymer chains, which resulted in slightly larger NGs (*ca*. 50 nm increase) compared to the specimens in PBS buffer. These observations were confirmed by the ζ-potential values: indeed, NGs showed an almost neutral charge at pH 4.5 and were negatively charged at pH 8.5[46-47].

AFM analysis (Figure 4c) was conducted in air on hydrated NGs and gave a diameter value of *ca.* 195 nm; the discrepancy between DLS and AFM measurements is attributable to the different measurement conditions: DLS analysis was performed on fully solvated NGs and the measured values corresponded to the NG hydrodynamic diameter, whereas for AFM measurements, a certain degree of dehydration is attributable to the experimental settings. Moreover, AFM conditions enhanced the typical Marangoni effect occurring in colloids: the crosslinked polymeric chains tend to spread according to the mass transfer driven by the surface tension gradient, induced by the variation in the evaporation flux across the surface of the laid droplet[48-49]. Due to this phenomenon, sample deposition procedure could result in colloidal agglomeration of NGs. In addition, SEM images (Figure 4d) showed a spherical morphology with a smooth surface and an approximate size around 114 nm. In this case, the smaller NG dimensions were related to the high-vacuum conditions, which led to a shrinking of the NG meshes due to the progressive transition from a swollen to a fully dehydrated state.

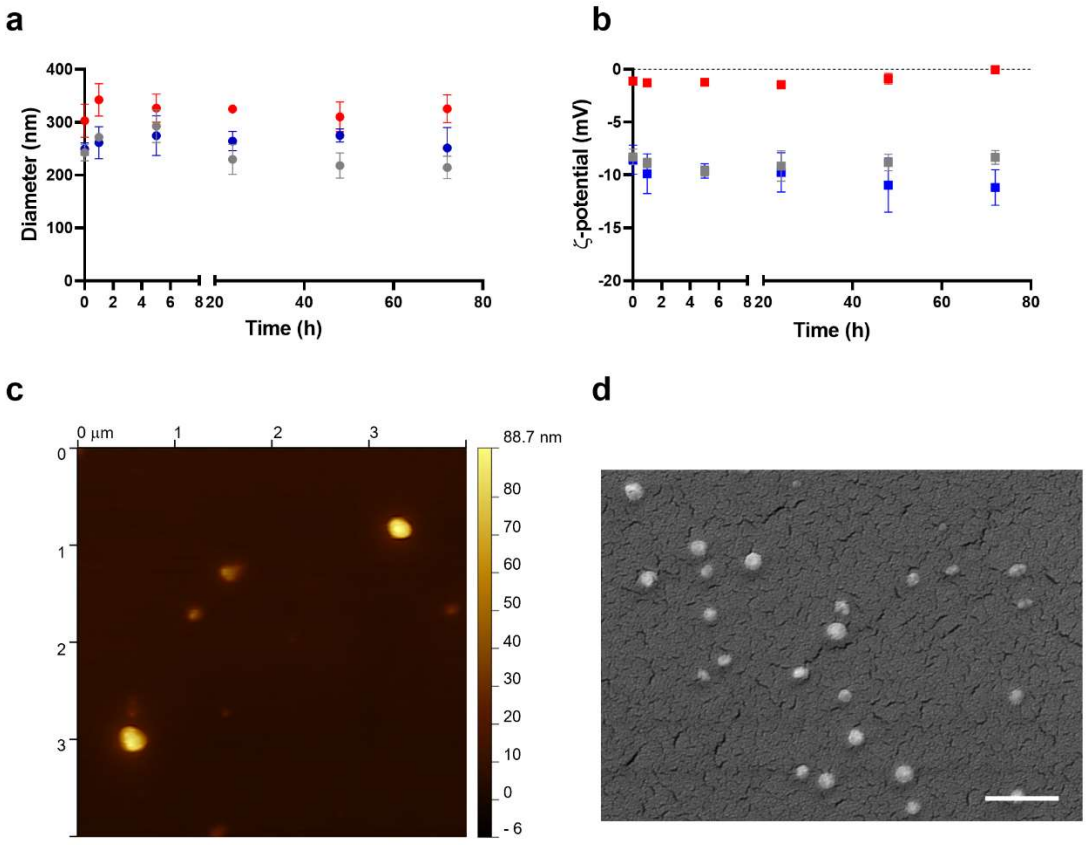

Figure 4. (a,b) Evaluation of NGs size and ζ-potential through DLS analysis in PBS (grey), acidic (red, pH 4.5) and alkaline (blue, pH 8.5) solutions. (c) AFM image of NGs. (d) SEM image of NGs. Scale bar = 500 nm.

Additionally, the enzymatic degradation of the nanocarrier was explored. HAase was chosen as a relevant enzyme, at two different concentrations (10 and 150 U/mL) commonly used in *in vitro* experiments[50-51], and the variation in NG size and morphology were evaluated through DLS and TEM analyses.

Results revealed a HAase dose-dependent degradation behavior of the NGs. Figure 5 shows the progressive decreases of the hydrodynamic diameter (up to 70% at 48 h) and the relative count rate for the specimen treated with HAase at the higher concentration (150 U/mL), highlighting the gradual degradation of the nanomaterial: in particular, the reduction in count rate is representative of the lower density of NGs in suspension, correlated to the decreased number of existing nanostructures[52-53]. Conversely, at 10 U/mL (a concentration giving an *in vitro* degradation rate

similar to the *in vivo* conditions[54]) the count rate decreased to an almost constant value. The reported increase in the NG size at 24 h might be attributed to an augmented swelling capacity due to the complete or partial cleavage of HA chains, which could generate local defects and nano-voids[52, 55]. However, in this case, NGs did not show a substantial degradation up to 48 h, suggesting a better stability of the nanocarrier for controlled drug delivery purposes (Supporting Information). Furthermore, TEM images confirmed DLS analysis (discrepancies in NG dimension could be attributed to the dry state of the specimens for TEM analysis), and showed the progressive alteration of NG morphology at 150 U/mL HAase solution, whereas the size of the NG treated with the enzymatic solution at 10 U/mL showed no significant reduction.

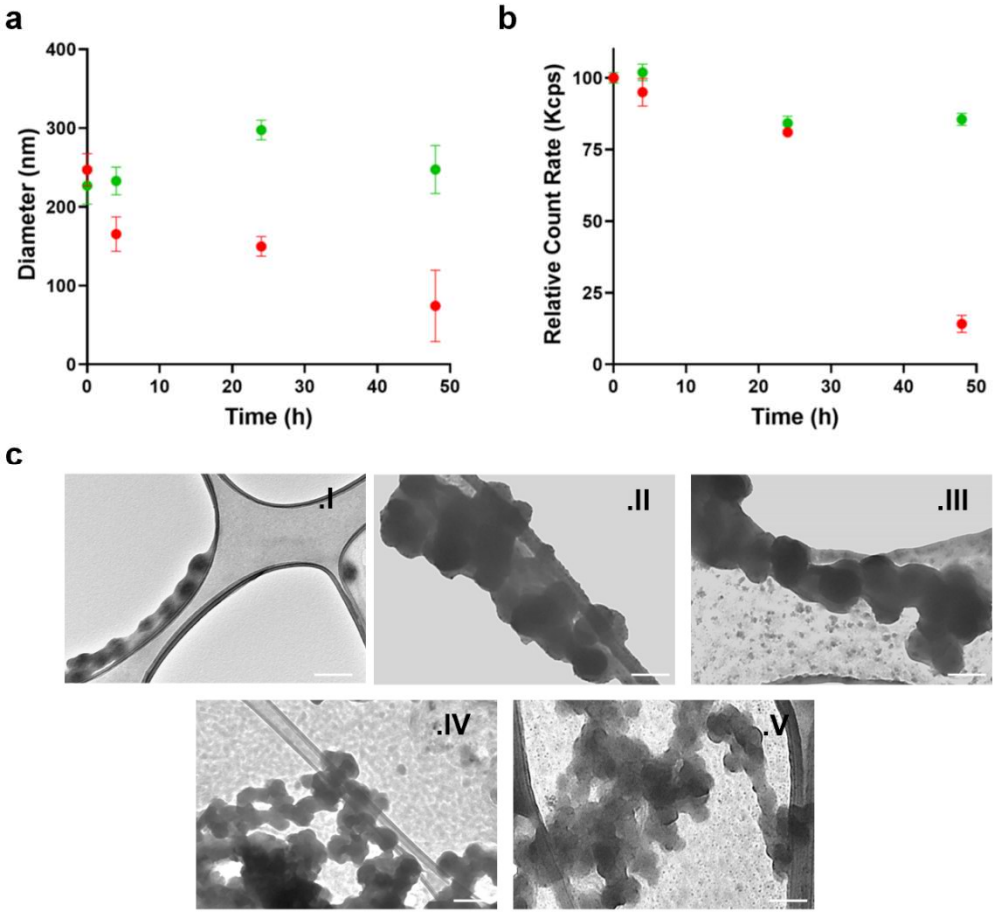

Figure 5. (a,b) DLS evaluation of NGs enzymatic degradation (size and relative count rate, respectively) in hyaluronidase solution 10 U/mL (green) and 150 U/mL (red). (c) Representative TEM images of NGs morphology in PBS solution (I, as-synthesized NGs) and following the treatments with HAase solution at 37 °C (II: 10 U/mL, 24 h; III: 10 U/mL, 48 h; IV: 150 U/mL, 24 h; V: 150 U/mL, 48 h). Scale bar = 250 nm.

Drug encapsulation and release

A key advantage of our NG system is the decoupling of the nanocarrier synthesis from the drug loading phase. Indeed, the synthesized nanocarriers can be stored as a lyophilized powder, until use. Subsequently, the selected drug can be encapsulated into the nanonetwork exploiting the NG sponge-like behavior (i.e., swelling behavior), thus obtaining a *ready-to-use* drug delivery system.

The performance of NGs as a controlled drug delivery system was investigated using DOX as a candidate drug. DOX is a cytotoxic anthracycline antibiotic commonly used in the treatment of several cancers, including lung[56], breast[57], melanoma[58], bladder[59] and ovarian[60] cancer. The DOX encapsulation efficiency was *ca.* 83.4%, as detected by fluorescence spectroscopy, and its release profiles in PBS, acidic and basic conditions are reported in Figure 6a. NGs exhibited a high encapsulation efficiency and a sustained drug delivery over time, showing a cumulative release of *ca*. 85% in PBS and an almost complete release at acidic and alkaline pH levels (*ca*. 93% and 97%, respectively), after 15 days. The trend in PBS could be ascribed to a diffusion mechanism mainly controlled by the aliphatic-aromatic stacking interactions between HA and DOX, as documented in systems where the high local density of atoms in aliphatic and aromatic rings can result in increased electrostatic and dispersive interactions, producing a stabilization effect[61-62]. Here, this phenomenon could take place between the aliphatic rings of the HA and the aromatic moieties of the drug, generating non-covalent interactions which provide a stacked arrangement of the drug molecules within the NGs architecture, reducing the release rate of DOX from the nanomatrix.

In acidic medium, NGs exhibited a drug release profile similar to that observed in PBS buffer up to 10 days, with an increase of the cumulative DOX release in the following days. Despite the larger NG size at pH 4.5 compared to PBS, the obtained result could be explained by considering the higher protonation degree of LPEI, which could lead to additional noncovalent interactions, of the class of cation-π interactions[63], between the protonated amine moieties of the polymer and the

aromatic rings of the drug. The physical nature of this interaction could contribute, together with the aliphatic-aromatic stacking, to tune the progressive release of DOX in the first days.

Alkaline conditions were characterized by the fastest release profile: this could be explained considering the increased negative charge on HA backbone, which may induce a repulsion between the carboxylate and hydroxide groups of HA and DOX, partially counteracting the interaction between the disaccharide units and the aromatic moiety of the drug, and resulting in an increased drug release from the nanomeshes.

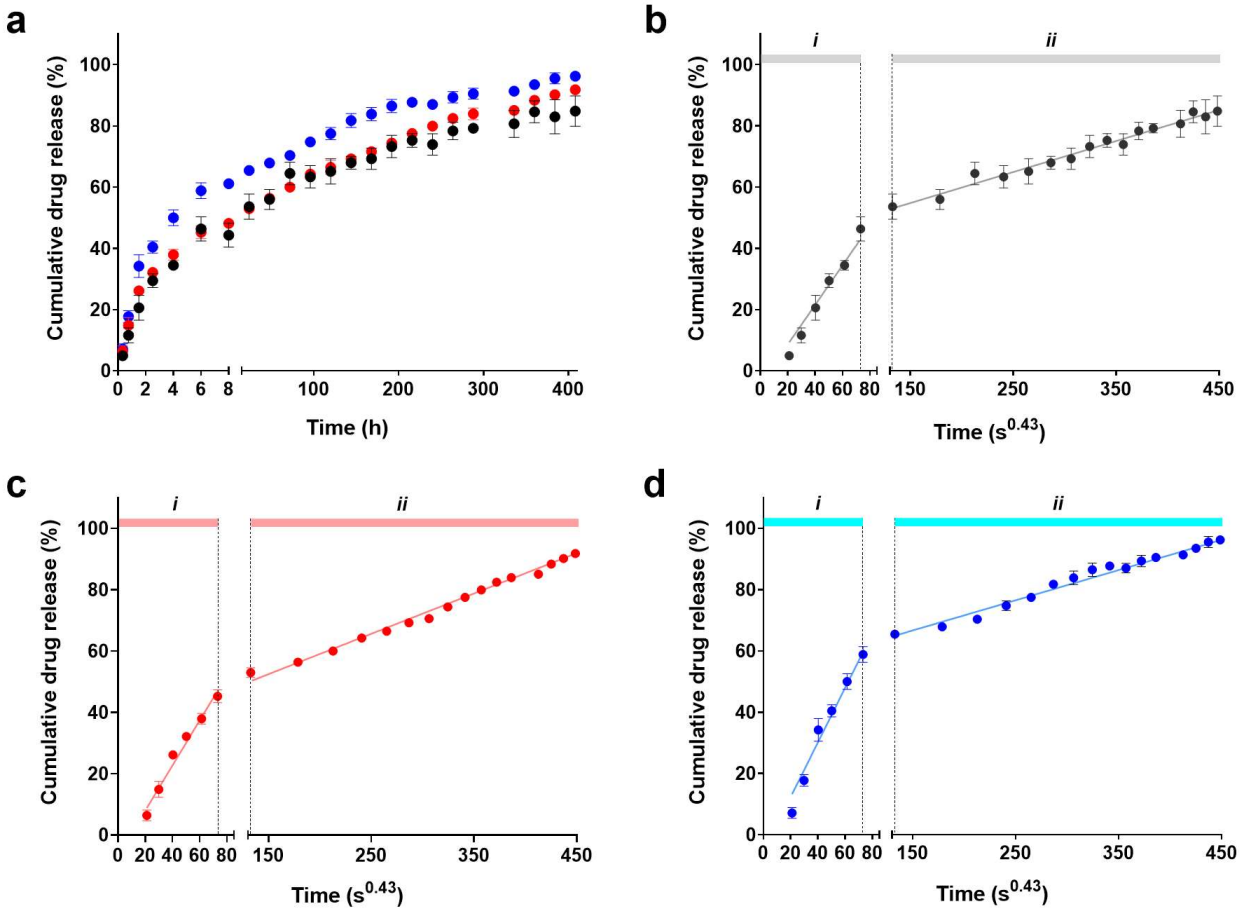

Figure 6. (a) Release profile of DOX delivered by NGs in PBS (black), acidic (pH = 4.5, red) and alkaline (pH = 8.5, blue) solutions. (b,c,d) The slope of the drug release against time expressed as $t^{1/2.3}$ is representative of the Fickian diffusion coefficient of drugs in NGs, at the different investigated conditions. Cumulative drug release is represented as a percentage of the total drug payload (mean value ± SD is plotted).

Figures 6b, 6c and 6d show the cumulative release against time to the power of 0.43 (i.e., $t^{1/2.3}$). In this representation, linearity of data is representative of a Fickian diffusion regime and the y-axis intercept value is an indication of the burst release, which is assumed equal to zero for an ideal controlled release system[35]. Collected data showed good linearity, confirming that DOX release was mediated by Fickian regime, and no initial burst release was noted, emphasizing the potential lifetime of this nanocarrier as a drug delivery system[64]. In particular, a double diffusion regime with different slopes was detected in all investigated conditions. The transition and duration of the two regimes could be ascribed to the nature of the predominant interactions drug-NGs over time. The first diffusion trend (*i*), occurring in the first 6 h, could be associated to the adsorbed DOX at the interface NGs/water, released at a faster rate according to the different pH values. The second regime (*ii*) could be due to the drug-NGs interactions in the nanoscaffold core, namely: the aliphatic-aromatic stacking causing delayed and sustained drug release in PBS; the aliphatic-aromatic and cation-π interactions prolonging drug release in acidic buffer; and the electrostatic repulsions counterbalancing the aliphatic-aromatic stacking for a faster DOX release in alkaline conditions.

NG biocompatibility

OVCA433 cells were chosen as a representative cell line expressing good affinity toward HA thanks to its high levels of CD44 expression (Supporting Information). Indeed, HA is considered the major ligand for CD44 and its isoforms in different cancer scenarios[65-66]. Proving the biocompatibility and the internalization of our NGs would highlight their potential use as therapeutic nanocarriers in ovarian cancer. G6PD assay demonstrated that HA-LPEI NGs did not generate cytotoxic effects on cells: Figure 7a reports high normalized viability levels (above 98%) with no significant difference *vs*. control (*i.e.*, cells without NGs).

NG internalization

To evaluate the involvement of CD44 in the NG internalization process, flow cytometric analysis of CD44-naïve and CD44-blocked OVCA433 following NG administration was conducted. Figure 7b shows the distribution of cell fluorescence at the investigated time points (2 h, 6 h and 24 h), where an increase of the MFI over time is representative of the progressive NG uptake by cells. A significantly different trend was observed in the two conditions: in control cells expressing CD44 surface receptors (–IM7), the uptake of the nanocarriers occurred over time and was clearly detectable at 24 h, with a 5.7-fold change in MFI; on the other hand, in cells treated with CD44 neutralizing/blocking antibody (+IM7), no relevant increase in MFI was observed and fluorescence histograms were comparable at all time points. These results demonstrate that CD44 was directly involved in the mechanism of NG internalization, supporting their potential use as a CD44-targeting drug delivery system. However, as recently discussed in the literature[67-68], this outcome should not be interpreted as a cell surface event of selective binding, because a rational approach to CD44 selective targeting through hyaluronan-based nanosystems is challenging: an unclear correlation between CD44 expression, HA binding and its internalization process does not allow CD44 to be assigned an exclusive role as a selective binder and internalizer in the uptake of HA-based nanomaterials.

A further validation of the internalization process was provided by fluorescence microscopy, as shown by the confocal images in Figure 7c, representative of the NG uptake at 24 h. Blocking CD44 receptors (+IM7) resulted in a substantial inhibition of NG uptake, while in CD44-naïve cells (–IM7), the nanocarriers were clearly detectable, with a progressive perinuclear localization (a 3D volume rendering of confocal z-stack is provided as Supporting Information).

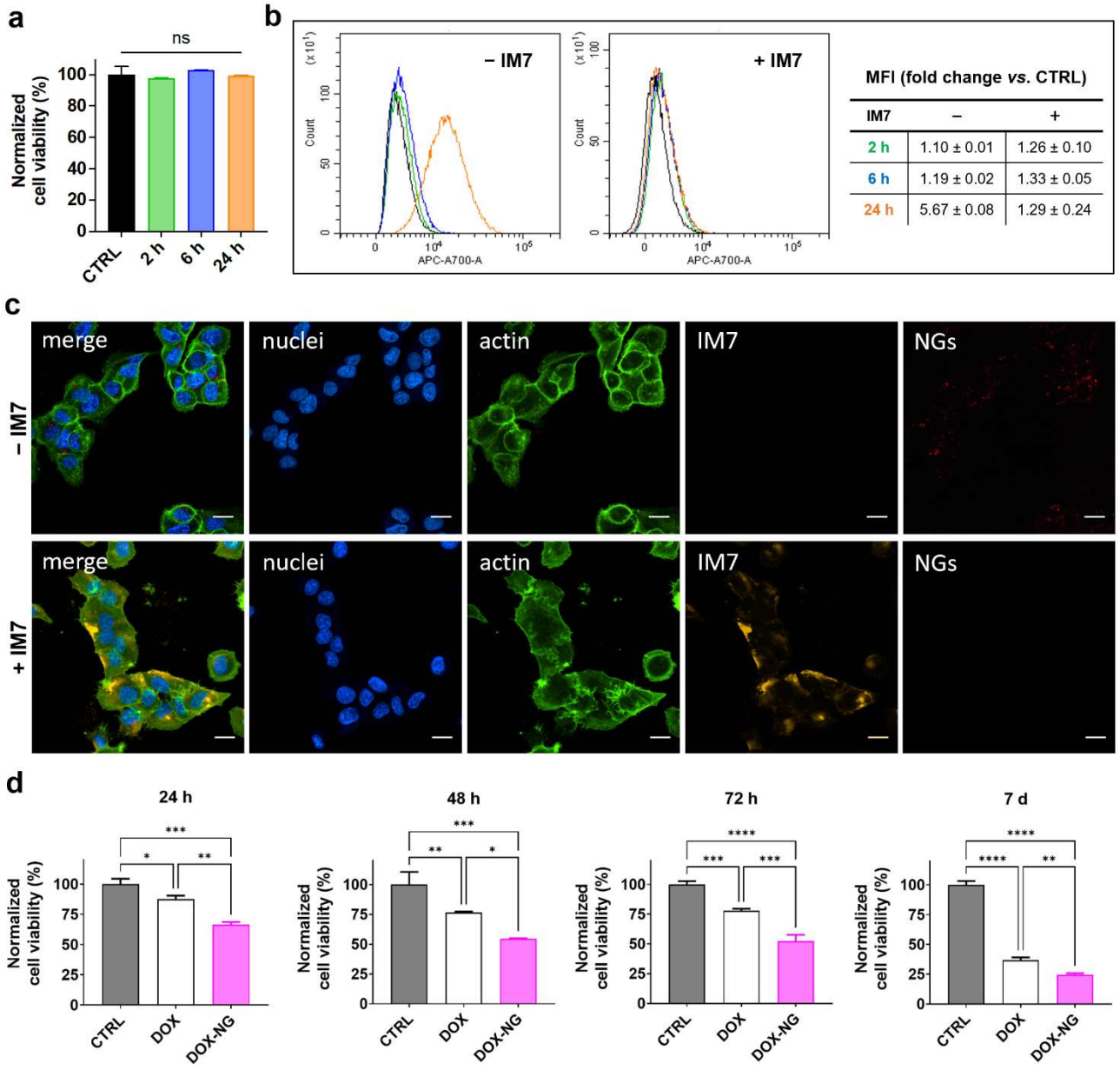

Figure 7. (a) Cell viability by G6PD assay of OVCA433 cells following incubation with NGs for 24 h. Results are normalized to CTRL group and expressed as mean ± SD. (b) Flow cytometric analysis of naïve OVCA433 (–IM7) vs. OVCA433 treated with CD44 neutralizing/blocking antibody (+IM7), after NGs uptake at 2 h (green), 6 h (blue) and 24 h (orange): plot reports the shift of the allophycocyanin (APC-A700-A) signal for each time point in the target gate (CTRL in black). The fold changes in MFI, calculated *vs.* internal control cells, are specified in the table. (c) Representative confocal micrographs of NGs (in red) internalization in OVCA433 cells after 24 h of incubation. NG internalization was not detectable in +IM7 group. Actin cytoskeleton was stained with FITC-labeled phalloidin and nuclei were counterstained with DAPI. Scale bar = 20 μm. (d) DOX-induced cytotoxicity in OVCA433 at 24 h, 48 h, 72 h and 7 days, after

the administration of free-drug (DOX) and drug-loaded NGs (DOX-NG). The therapeutic effect is expressed in terms of cell viability levels normalized against internal controls, measured through the MTT assay. Results are the mean ± SD of three independent experiments. Statistical analysis was performed using one-way ANOVA. * $p < 0.05$, ** $p < 0.01$, **** $p < 0.001$, **** $p < 0.0001$, ns = not significant.

Effect of NGs-mediated release of DOX on cells

To validate our NG formulation, we performed an *in vitro* evaluation of the therapeutic effects of NG-mediated DOX release, comparing the nanoencapsulation approach to the conventional administration route of the pristine drug. We selected an ideal sublethal drug concentration of 0.2 μM, corresponding to a 14% cell viability reduction, as estimated through the dose-response curve at 24 h on OVCA433 cultured in adhesion, using the MTT assay (Supporting Information). This drug concentration falls in the range of values commonly investigated for ovarian cancer treatments[69-70]. The cell metabolic activity was estimated through MTT assay, up to 7 days, as reported in Figure 7d. The administration of DOX-loaded NGs (DOX-NG) boosted the therapeutic effect of the drug, as clearly detectable after 24 h ($p<0.0001$ *vs.* CTRL), outperforming the non-encapsulated DOX ($p<0.01$ *vs.* DOX). Moreover, the sustained drug release ensured prolonged effects on cell metabolism over time, with a constantly improved performance vs. the conventional drug administration route, leaving a low residual cell viability at 1 week ($p<0.0001$ *vs.* CTRL and $p<0.01$ *vs.* DOX).

Overall, these results offer a new perspective on the synthesis of NGs *via* MEET, overcoming the limitations in the design of nanoscaffolds related to the use of organic-insoluble adducts, and resulting in a biocompatible nanomaterial system with enhanced drug delivery performances for pharmacological therapies.

Conclusions

In this work, we propose a novel method (MEET) to synthesize NGs based on the HA-LPEI system, which is not suitable for conventional emulsion syntheses due to the hydrophilic nature of the two polymers. The design of a mixed emulsion strategy allows the hydrophilic polymers to constitute different dispersed aqueous phases, capable of interacting at their interface to activate the NG crosslinking reaction. This obviates the need for a hydrophobic polymeric counterpart, as required in the conventional W/O emulsification/evaporation method. The resulting NGs were validated for the controlled release of doxorubicin, a common anticancer drug, demonstrating a high drug loading capability and a sustained release over time. Choosing ovarian cancer as a model, we demonstrated the involvement of the hyaluronan receptor CD44 in the NG internalization process, by showing that the selective CD44 blockade resulted in a significant inhibition of NG uptake. This underlines the CD44-targeting ability of the developed nanosystem. Additionally, DOX-loaded NGs exhibited an enhanced therapeutic effect outperforming the conventional non-encapsulated drug administration route, even at sublethal dosages.

Overall, our results suggest that HA-LPEI NGs may represent a promising targeted drug delivery system in ovarian cancer. Additionally, the proposed MEET approach, overcoming the major limitations of the standard emulsion/evaporation technique, has the potential to offer a new route for the design of smart NGs for cancer therapy.

Supporting Information

Evaluation of optimal LPEI level in NG formulation; DOX calibration curves in acidic, PBS, and basic solutions; DLS analysis of drug-loaded NGs; DOX calibration curve and NG-mediated drug release profiles in HAase solutions (10 U/mL and 150 U/mL); OVCA433 Western Blotting; 3D rendering of NGs internalization; dose-response curve of DOX.

Author Contributions

The manuscript was written through contributions of all authors. E.L.: Investigation, Formal analysis, Visualization, Writing - Original Draft; P.M., S.M.G., F.P., X.H.: Investigation; Formal analysis; D.D.R., F.A., F.B.: Investigation; L.R.: Supervision, Funding acquisition; S.S.: Supervision, Writing - Review & Editing; M.T., G.G., Z.J.Z.: Supervision, Resources; E.M.: Conceptualization, Methodology, Validation, Formal analysis, Visualization, Writing - Original Draft, Writing - Review & Editing; A.R.: Supervision, Methodology, Validation, Writing - Original Draft, Writing - Review & Editing, Funding acquisition.

All authors have given approval to the final version of the manuscript.

Acknowledgments

This work has been partially supported by Regione Lazio – POR FESR Lazio 2014-2020 “Gruppi di Ricerca 2020”, proposal ID A0375-2020-36596 (ORGANOVA), CUP: B85F21001500002.

P.M., G.G. and A.R. are thankful to “Tecnopolo per la medicina di precisione” (TecnoMed Puglia) - Regione Puglia: DGR n.2117 dated 21/11/2018, CUP: B84I18000540002 and “Tecnopolo di Nanotecnologia e Fotonica per la Medicina di Precisione” (TECNOMED) - FISR/MIUR- CNR: delibera CIPE n.3449 dated 07/08/2017, CUP: B83B17000010001.

References

(1) Mauri, E.; Giannitelli, S. M.; Trombetta, M.; Rainer, A. Synthesis of Nanogels: Current Trends and Future Outlook. *Gels* **2021,** *7* (2), 36, DOI: 10.3390/gels7020036.

(2) Neamtu, I.; Rusu, A. G.; Diaconu, A.; Nita, L. E.; Chiriac, A. P. Basic concepts and recent advances in nanogels as carriers for medical applications. *Drug Deliv* **2017,** *24* (1), 539-557, DOI: 10.1080/10717544.2016.1276232.

(3) Soni, G.; Yadav, K. S. Nanogels as potential nanomedicine carrier for treatment of cancer: A mini review of the state of the art. *Saudi Pharma J* **2016,** *24* (2), 133-139, DOI: 10.1016/j.jsps.2014.04.001.

(4) Qureshi, M. A.; Khatoon, F. Different types of smart nanogel for targeted delivery. *J Sci: Adv Mater Devices* **2019,** *4* (2), 201-212, DOI: 10.1016/j.jsamd.2019.04.004.

(5) Mauri, E.; Perale, G.; Rossi, F. Nanogel Functionalization: A Versatile Approach To Meet the Challenges of Drug and Gene Delivery. *ACS Appl Nano Mater* **2018,** *1* (12), 6525-6541, DOI: 10.1021/acsanm.8b01686.

(6) Wang, Y.; Li, P.; Truong-Dinh Tran, T.; Zhang, J.; Kong, L. Manufacturing Techniques and Surface Engineering of Polymer Based Nanoparticles for Targeted Drug Delivery to Cancer. *Nanomaterials (Basel)* **2016,** *6* (2), 26, DOI: 10.3390/nano6020026.

(7) Vinogradov, S. V.; Zeman, A. D.; Batrakova, E. V.; Kabanov, A. V. Polyplex Nanogel formulations for drug delivery of cytotoxic nucleoside analogs. *J Control Release* **2005,** *107* (1), 143-157, DOI: 10.1016/j.jconrel.2005.06.002.

(8) Papa, S.; Veneruso, V.; Mauri, E.; Cremonesi, G.; Mingaj, X.; Mariani, A.; De Paola, M.; Rossetti, A.; Sacchetti, A.; Rossi, F.; Forloni, G.; Veglianese, P. Functionalized nanogel for treating activated astrocytes in spinal cord injury. *J Control Release* **2021,** *330*, 218-228, DOI: 10.1016/j.jconrel.2020.12.006.

(9) Vinogradov, S. V.; Kohli, E.; Zeman, A. D. Comparison of Nanogel Drug Carriers and their Formulations with Nucleoside 5′-Triphosphates. *Pharm Res* **2006,** *23* (5), 920-930, DOI: 10.1007/s11095-006-9788-5.

(10) Reddy Hv, R.; Bhattacharyya, S. In vitro evaluation of mucoadhesive in situ nanogel of celecoxib for buccal delivery. *Ann Pharm Fr* **2021,** *79* (4), 418-430, DOI: 10.1016/j.pharma.2021.01.006.

(11) Tripodo, G.; Trapani, A.; Torre, M. L.; Giammona, G.; Trapani, G.; Mandracchia, D. Hyaluronic acid and its derivatives in drug delivery and imaging: Recent advances and challenges. *Eur J Pharm Biopharm* **2015,** *97*, 400-416, DOI: 10.1016/j.ejpb.2015.03.032.

(12) Vasvani, S.; Kulkarni, P.; Rawtani, D. Hyaluronic acid: A review on its biology, aspects of drug delivery, route of administrations and a special emphasis on its approved marketed products and recent clinical studies. *Int J Biol Macromol* **2020,** *151*, 1012-1029, DOI: 10.1016/j.ijbiomac.2019.11.066.

(13) Luo, Z.; Dai, Y.; Gao, H. Development and application of hyaluronic acid in tumor targeting drug delivery. *Acta Pharm Sin B* **2019,** *9* (6), 1099-1112, DOI:10.1016/j.apsb.2019.06.004.

(14) Karbownik, M. S.; Nowak, J. Z. Hyaluronan: Towards novel anti-cancer therapeutics. *Pharmacol Rep* **2013,** *65* (5), 1056-1074, DOI: 10.1016/S1734-1140(13)71465-8.

(15) Cheng, X.; Shi, S.; Wu, Y.; Zhu, L.; Xu, J.; Hu, T.; Wei, B.; Tang, R. Cisplatin-Cross-Linked and Oxygen-Resupply Hyaluronic Acid-Based Nanocarriers for Chemo-photodynamic Therapy. *ACS Appl Nano Mater* **2021**, DOI: 10.1021/acsanm.1c01662.

(16) Zou, Y.; Li, D.; Shen, M.; Shi, X. Polyethylenimine-Based Nanogels for Biomedical Applications. *Macromol Biosci* **2019,** *19* (11), 1900272, DOI: 10.1002/mabi.201900272.

(17) Bus, T.; Traeger, A.; Schubert, U. S. The great escape: how cationic polyplexes overcome the endosomal barrier. *J Mater Chem B* **2018,** *6* (43), 6904-6918, DOI: 10.1039/C8TB00967H.

(18) Yu, K.; Zhao, J.; Yu, C.; Sun, F.; Liu, Y.; Zhang, Y.; Lee, R. J.; Teng, L.; Li, Y. Role of Four Different Kinds of Polyethylenimines (PEIs) in Preparation of Polymeric Lipid Nanoparticles and Their Anticancer Activity Study. *J Cancer* **2016,** *7* (7), 872-882, DOI: 10.7150/jca.13855.

(19) Sahiner, N.; Sagbas, S.; Sahiner, M.; Ayyala, R. S. Polyethyleneimine modified poly(Hyaluronic acid) particles with controllable antimicrobial and anticancer effects. *Carbohydr Polym* **2017,** *159*, 29-38, DOI: 10.1016/j.carbpol.2016.12.024.

(20) Zhu, Y.; Wang, Y.; Sun, Y.; Shen, J.; Xu, J.; Chai, Y.; Yang, Y. In situ self imine-crosslinked nanocomplexes loaded with small noncoding RNA for efficient osteoarthritis attenuation. *Chem Eng J* **2021,** *420*, 127631, DOI: 10.1016/j.cej.2020.127631.

(21) Chen, C.; Zhou, B.; Zhu, X.; Shen, M.; Shi, X. Branched polyethyleneimine modified with hyaluronic acid via a PEG spacer for targeted anticancer drug delivery. *Rsc Adv* **2016,** *6* (11), 9232-9239, DOI: 10.1039/C5RA23022E.

(22) Wang, S.; Zhang, J.; Wang, Y.; Chen, M. Hyaluronic acid-coated PEI-PLGA nanoparticles mediated co-delivery of doxorubicin and miR-542-3p for triple negative breast cancer therapy. *Nanomed: Nanotechnol Biol Med* **2016,** *12* (2), 411-420, DOI: 10.1016/j.nano.2015.09.014.

(23) Xu, Y.; Liu, D.; Hu, J.; Ding, P.; Chen, M. Hyaluronic acid-coated pH sensitive poly (β-amino ester) nanoparticles for co-delivery of embelin and TRAIL plasmid for triple negative breast cancer treatment. *Int J Pharm* **2020,** *573*, 118637, DOI: 10.1016/j.ijpharm.2019.118637.

(24) Zheng, X.; Zhang, F.; Zhao, Y.; Zhang, J.; Dawulieti, J.; Pan, Y.; Cui, L.; Sun, M.; Shao, D.; Li, M.; He, K.; Zhang, M.; Li, J.; Chen, L. Self-assembled dual fluorescence nanoparticles for CD44-targeted delivery of anti-miR-27a in liver cancer theranostics. *Theranostics* **2018,** *8* (14), 3808-3823, DOI: 10.7150/thno.25255.

(25) Park, J. S.; Yi, S. W.; Kim, H. J.; Park, K.-H. Receptor-mediated gene delivery into human mesenchymal stem cells using hyaluronic acid-shielded polyethylenimine/pDNA nanogels. *Carbohydr Polym* **2016,** *136*, 791-802, DOI: 10.1016/j.carbpol.2015.09.053.

(26) Fortuni, B.; Inose, T.; Ricci, M.; Fujita, Y.; Van Zundert, I.; Masuhara, A.; Fron, E.; Mizuno, H.; Latterini, L.; Rocha, S.; Uji-i, H. Polymeric Engineering of Nanoparticles for Highly Efficient Multifunctional Drug Delivery Systems. *Sci Rep-Uk* **2019,** *9* (1), 2666, DOI: 10.1038/s41598-019-39107-3.

(27) Mauri, E.; Veglianese, P.; Papa, S.; Mariani, A.; De Paola, M.; Rigamonti, R.; Chincarini, Giulia M. F.; Vismara, I.; Rimondo, S.; Sacchetti, A.; Rossi, F. Double conjugated nanogels for selective intracellular drug delivery. *Rsc Adv* **2017,** *7* (48), 30345-30356, DOI: 10.1039/C7RA04584K.

(28) Pizzetti, F.; Maspes, A.; Rossetti, A.; Rossi, F. The addition of hyaluronic acid in chemical hydrogels can tune the physical properties and degradability. *Eur Polym J* **2021,** *161*, 110843, DOI: 10.1016/j.eurpolymj.2021.110843.

(29) Kolayli, S.; Sahin, H.; Can, Z.; Yildiz, O.; Sahin, K. Honey shows potent inhibitory activity against the bovine testes hyaluronidase. *J Enzyme Inhib Med Chem* **2016,** *31* (4), 599-602, DOI: 10.3109/14756366.2015.1054819.

(30) Demitrack, E. S.; Aihara, E.; Kenny, S.; Varro, A.; Montrose, M. H. Inhibitors of acid secretion can benefit gastric wound repair independent of luminal pH effects on the site of damage. *Gut* **2012,** *61* (6), 804-811, DOI: 10.1136/gutjnl-2011-300420.

(31) Khan, M. Z. I.; Prebeg, Ž.; Kurjaković, N. A pH-dependent colon targeted oral drug delivery system using methacrylic acid copolymers: I. Manipulation of drug release using Eudragit® L100-55 and Eudragit® S100 combinations. *J Control Release* **1999,** *58* (2), 215-222, DOI: 10.1016/S0168-3659(98)00151-5.

(32) Elbert, D. L. Liquid–liquid two-phase systems for the production of porous hydrogels and hydrogel microspheres for biomedical applications: A tutorial review. *Acta Biomater* **2011,** *7* (1), 31-56, DOI: 10.1016/j.actbio.2010.07.028.

(33) Sheth, T.; Seshadri, S.; Prileszky, T.; Helgeson, M. E. Multiple nanoemulsions. *Nat Rev Mater* **2020,** *5* (3), 214-228, DOI: 10.1038/s41578-019-0161-9.

(34) Hack, M. A.; Vondeling, P.; Cornelissen, M.; Lohse, D.; Snoeijer, J. H.; Diddens, C.; Segers, T. Asymmetric coalescence of two droplets with different surface tensions is caused by capillary waves. *Phys Rev Fluids* **2021,** *6* (10), 104002, DOI: 10.1103/PhysRevFluids.6.104002.

(35) Mauri, E.; Gori, M.; Giannitelli, S. M.; Zancla, A.; Mozetic, P.; Abbruzzese, F.; Merendino, N.; Gigli, G.; Rossi, F.; Trombetta, M.; Rainer, A. Nano-encapsulation of hydroxytyrosol into formulated nanogels improves therapeutic effects against hepatic steatosis: An in vitro study. *Mater Sci Eng C* **2021,** *124*, 112080, DOI: 10.1016/j.msec.2021.112080.

(36) Son, G. M.; Kim, H. Y.; Ryu, J. H.; Chu, C. W.; Kang, D. H.; Park, S. B.; Jeong, Y.-I. Self-assembled polymeric micelles based on hyaluronic acid-g-poly(D,L-lactide-co-glycolide) copolymer for tumor targeting. *Int J Mol Sci* **2014,** *15* (9), 16057-16068, DOI: 10.3390/ijms150916057.

(37) Zhou, B.; Zheng, L.; Peng, C.; Li, D.; Li, J.; Wen, S.; Shen, M.; Zhang, G.; Shi, X. Synthesis and Characterization of PEGylated Polyethylenimine-Entrapped Gold Nanoparticles for Blood Pool and Tumor CT Imaging. *ACS Appl Mater Interfaces* **2014,** *6* (19), 17190-17199, DOI: 10.1021/am505006z.

(38) Quiñones, J. P.; Brüggemann, O.; Covas, C. P.; Ossipov, D. A. Self-assembled hyaluronic acid nanoparticles for controlled release of agrochemicals and diosgenin. *Carbohydr Polym* **2017,** *173*, 157-169, DOI: 10.1016/j.carbpol.2017.05.048.

(39) Shah, C. B.; Barnett, S. M. Swelling behavior of hyaluronic acid gels. *J Appl Polym Sci* **1992,** *45* (2), 293-298, DOI: 10.1002/app.1992.070450211.

(40) Dong, Q.; Guo, X.; Li, L.; Yu, C.; Nie, L.; Tian, W.; Zhang, H.; Huang, S.; Zang, H. Understanding hyaluronic acid induced variation of water structure by near-infrared spectroscopy. *Sci Rep-Uk* **2020,** *10* (1), 1387, DOI: 10.1038/s41598-020-58417-5.

(41) Collins, M. N.; Birkinshaw, C. Investigation of the swelling behavior of crosslinked hyaluronic acid films and hydrogels produced using homogeneous reactions. *J Appl Polym Sci* **2008,** *109* (2), 923-931, DOI: 10.1002/app.27631.

(42) Neu, M.; Fischer, D.; Kissel, T. Recent advances in rational gene transfer vector design based on poly(ethylene imine) and its derivatives. *J Gene Med* **2005,** *7* (8), 992-1009, DOI: 10.1002/jgm.773.

(43) Mauri, E.; Chincarini, G. M. F.; Rigamonti, R.; Magagnin, L.; Sacchetti, A.; Rossi, F. Modulation of electrostatic interactions to improve controlled drug delivery from nanogels. *Mater Sci Eng C* **2017,** *72*, 308-315, DOI: 10.1016/j.msec.2016.11.081.

(44) Lapčík, L.; Lapčík, L.; De Smedt, S.; Demeester, J.; Chabreček, P. Hyaluronan: Preparation, Structure, Properties, and Applications. *Chem Rev* **1998,** *98* (8), 2663-2684, DOI: 10.1021/cr941199z.

(45) Welti, D.; Rees, D. A.; Welsh, E. J. Solution Conformation of Glycosaminoglycans: Assignment of the 300-MHz 1H-Magnetic Resonance Spectra of Chondroitin 4-Sulphate, Chondroitin 6-Sulphate and Hyaluronate, and Investigation of an Alkali-Induced Conformation Change. *Eur J Biochem* **1979,** *94* (2), 505-514, DOI: 10.1111/j.1432-1033.1979.tb12919.x.

(46) Ghosh, S.; Kobal, I.; Zanette, D.; Reed, W. F. Conformational contraction and hydrolysis of hyaluronate in sodium hydroxide solutions. *Macromolecules* **1993,** *26* (17), 4685-4693, DOI: 10.1021/ma00069a042.

(47) Gribbon, P.; Heng, B. C.; Hardingham, T. E. The Molecular Basis of the Solution Properties of Hyaluronan Investigated by Confocal Fluorescence Recovery After Photobleaching. *Biophys J* **1999,** *77* (4), 2210-2216, DOI: 10.1016/S0006-3495(99)77061-X.

(48) Ren, J.; Crivoi, A.; Duan, F. Disk-Ring Deposition in Drying a Sessile Nanofluid Droplet with Enhanced Marangoni Effect and Particle Surface Adsorption. *Langmuir* **2020,** *36* (49), 15064-15074, DOI: 10.1021/acs.langmuir.0c02607.

(49) Su, R.; Park, S. H.; Li, Z.; McAlpine, M. C. 13 - 3D printed electronic materials and devices. In *Robotic Systems and Autonomous Platforms*; Walsh, S. M.; Strano, M. S., Eds.; Woodhead Publishing: 2019; pp 309-334.

(50) Ding, J.; Liang, T.; Zhou, Y.; He, Z.; Min, Q.; Jiang, L.; Zhu, J. Hyaluronidase-triggered anticancer drug and siRNA delivery from cascaded targeting nanoparticles for drug-resistant breast cancer therapy. *Nano Res* **2017,** *10* (2), 690-703, DOI: 10.1007/s12274-016-1328-y.

(51) Yeo, Y.; Bellas, E.; Highley, C. B.; Langer, R.; Kohane, D. S. Peritoneal adhesion prevention with an in situ cross-linkable hyaluronan gel containing tissue-type plasminogen activator in a rabbit repeated-injury model. *Biomaterials* **2007,** *28* (25), 3704-3713, DOI: 10.1016/j.biomaterials.2007.04.033.

(52) Wei, P.; Gangapurwala, G.; Pretzel, D.; Leiske, M. N.; Wang, L.; Hoeppener, S.; Schubert, S.; Brendel, J. C.; Schubert, U. S. Smart pH-Sensitive Nanogels for Controlled Release in an Acidic Environment. *Biomacromolecules* **2019,** *20* (1), 130-140, DOI: 10.1021/acs.biomac.8b01228.

(53) Schmitz, D.; Pich, A. Responsive microgels with supramolecular crosslinks: synthesis and triggered degradation in aqueous medium. *Polym Chem* **2016,** *7* (36), 5687-5697, DOI: 10.1039/C6PY01039C.

(54) Bajaj, G.; Kim, M. R.; Mohammed, S. I.; Yeo, Y. Hyaluronic acid-based hydrogel for regional delivery of paclitaxel to intraperitoneal tumors. *J Control Release* **2012,** *158* (3), 386-392, DOI: 10.1016/j.jconrel.2011.12.001.

(55) Hoelscher, F.; Machado, T. O.; de Oliveira, D.; Hermes de Araújo, P. H.; Sayer, C. Enzymatically catalyzed degradation of poly (thioether-ester) nanoparticles. *Polym Degrad Stab* **2018,** *156*, 211-217, DOI: 10.1016/j.polymdegradstab.2018.09.007.

(56) Hong, Y.; Che, S.; Hui, B.; Yang, Y.; Wang, X.; Zhang, X.; Qiang, Y.; Ma, H. Lung cancer therapy using doxorubicin and curcumin combination: Targeted prodrug based, pH sensitive nanomedicine. *Biomed Pharmacother* **2019,** *112*, 108614, DOI: 10.1016/j.biopha.2019.108614.

(57) Zheng, G.; Zheng, M.; Yang, B.; Fu, H.; Li, Y. Improving breast cancer therapy using doxorubicin loaded solid lipid nanoparticles: Synthesis of a novel arginine-glycine-aspartic tripeptide conjugated, pH sensitive lipid and evaluation of the nanomedicine in vitro and in vivo. *Biomed Pharmacother* **2019,** *116*, 109006, DOI: 10.1016/j.biopha.2019.109006.

(58) Capanema, N. S. V.; Carvalho, I. C.; Mansur, A. A. P.; Carvalho, S. M.; Lage, A. P.; Mansur, H. S. Hybrid Hydrogel Composed of Carboxymethylcellulose–Silver Nanoparticles–Doxorubicin for Anticancer and Antibacterial Therapies against Melanoma Skin Cancer Cells. *ACS Appl Nano Mater* **2019,** *2* (11), 7393-7408, DOI: 10.1021/acsanm.9b01924.

(59) Chung, D. Y.; Kang, D. H.; Kim, J. W.; Ha, J. S.; Kim, D. K.; Cho, K. S. Comparison of Oncologic Outcomes of Dose-Dense Methotrexate, Vinblastine, Doxorubicin, and Cisplatin (ddMVAC) with Gemcitabine and Cisplatin (GC) as Neoadjuvant Chemotherapy for Muscle-Invasive Bladder Cancer: Systematic Review and Meta-Analysis. *Cancers* **2021,** *13* (11), 2770, DOI: 10.3390/cancers13112770.

(60) Eetezadi, S.; Evans, J. C.; Shen, Y.-T.; De Souza, R.; Piquette-Miller, M.; Allen, C. Ratio-Dependent Synergism of a Doxorubicin and Olaparib Combination in 2D and Spheroid Models of Ovarian Cancer. *Mol Pharm* **2018,** *15* (2), 472-485, DOI: 10.1021/acs.molpharmaceut.7b00843.

(61) Ninković, D. B.; Vojislavljević-Vasilev, D. Z.; Medaković, V. B.; Hall, M. B.; Brothers, E. N.; Zarić, S. D. Aliphatic–aromatic stacking interactions in cyclohexane–benzene are stronger than aromatic–aromatic interaction in the benzene dimer. *Phys Chem Chem Phys* **2016,** *18* (37), 25791-25795, DOI: 10.1039/C6CP03734H.

(62) Cabaleiro-Lago, E. M.; Rodríguez-Otero, J. On the Nature of σ–σ, σ–π, and π–π Stacking in Extended Systems. *ACS Omega* **2018,** *3* (8), 9348-9359, DOI: 10.1021/acsomega.8b01339.

(63) Ma, J. C.; Dougherty, D. A. The Cation−π Interaction. *Chem Rev* **1997,** *97* (5), 1303-1324, DOI: 10.1021/cr9603744.

(64) Huang, X.; Brazel, C. S. On the importance and mechanisms of burst release in matrix-controlled drug delivery systems. *J Control Release* **2001,** *73* (2), 121-136, DOI: 10.1016/S0168-3659(01)00248-6.

(65) Senbanjo, L. T.; Chellaiah, M. A. CD44: A Multifunctional Cell Surface Adhesion Receptor Is a Regulator of Progression and Metastasis of Cancer Cells. *Cell Dev Biol* **2017,** *5* (18), DOI: 10.3389/fcell.2017.00018.

(66) Price, Z. K.; Lokman, N. A.; Ricciardelli, C. Differing Roles of Hyaluronan Molecular Weight on Cancer Cell Behavior and Chemotherapy Resistance. *Cancers* **2018,** *10* (12), 482, DOI: 10.3390/cancers10120482.

(67) Rios de la Rosa, J. M.; Pingrajai, P.; Pelliccia, M.; Spadea, A.; Lallana, E.; Gennari, A.; Stratford, I. J.; Rocchia, W.; Tirella, A.; Tirelli, N. Binding and Internalization in Receptor-Targeted Carriers: The Complex Role of CD44 in the Uptake of Hyaluronic Acid-Based Nanoparticles (siRNA Delivery). *Adv Healthc Mater* **2019,** *8* (24), 1901182, DOI: 10.1002/adhm.201901182.

(68) Tirella, A.; Kloc-Muniak, K.; Good, L.; Ridden, J.; Ashford, M.; Puri, S.; Tirelli, N. CD44 targeted delivery of siRNA by using HA-decorated nanotechnologies for KRAS silencing in cancer treatment. *Int J Pharm* **2019,** *561*, 114-123, DOI: 10.1016/j.ijpharm.2019.02.032.

(69) Tang, Y.; McGoron, A. J. Combined effects of laser-ICG photothermotherapy and doxorubicin chemotherapy on ovarian cancer cells. *J Photochem Photobiol B* **2009,** *97* (3), 138-144, DOI: 10.1016/j.jphotobiol.2009.09.001.

(70) Norouzi-Barough, L.; Sarookhani, M.; Salehi, R.; Sharifi, M.; Moghbelinejad, S. CRISPR/Cas9, a new approach to successful knockdown of ABCB1/P-glycoprotein and reversal of chemosensitivity in human epithelial ovarian cancer cell line. *Iran J Basic Med Sci* **2018,** *21* (2), 181-187, DOI: 10.22038/IJBMS.2017.25145.6230.